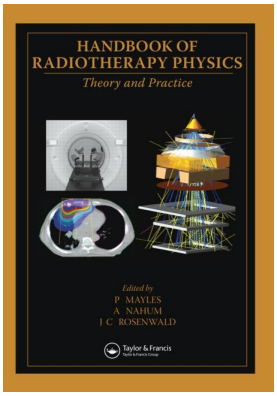

Handbook of Radiotherapy Physics
Theory and Practice

P. Mayles, A. Nahum, J. C. Rosenwald

Interactions of Charged Particles with Matter

Publication details
https://test.routledgehandbooks.com/doi/10.1201/9781420012026.ch3
Alan Nahum
Published online on: 12 Jun 2007

CHAPTER 3

INTERACTIONS OF CHARGED PARTICLES WITH MATTER

Alan Nahum

CONTENTS

3.1 INTRODUCTION

Charged particles are fundamental to the medical use of radiation. Even if the primary radiation is a photon beam, it is the charged particles, known as secondary radiation in such cases, that cause the biological effect, whether it be cell killing or other changes that may eventually induce cancer. In fact, charged particles are often termed *ionising* radiation, and photons (and neutrons) termed *non-ionising* or *indirectly ionising*. Furthermore, a precise knowledge of the *spatial* distribution of the absorbed dose is crucial to radiotherapy treatment planning and delivery (and in certain cases, to radiation protection considerations), and this can only be obtained if the transport of the energy by the charged particles (overwhelmingly electrons) can be modelled. In many cases, the ranges of, for example, the Compton electrons (see Section 4.3.2) generated by megavoltage x-ray beams are appreciable (up to several cm) and must, therefore, be accurately modelled. The generation of x-rays, i.e. bremsstrahlung, is a charged-particle interaction. Alternatively, radiotherapy is sometimes delivered by primary charged particle beams, usually megavoltage electrons, where electron interactions with matter are obviously crucial. However, increasingly, proton beams are coming into therapeutic use (see Chapter 46), and even so-called heavy ions such as carbon are used (see Chapter 49). Mention can also be made of unsealed source therapy (Part K) with, for example, β-emitting radionuclides; these electrons (or positrons) can also have ranges up to a centimetre. The subject of radiation dosimetry (see Chapter 6 and Part D) depends on an intimate knowledge of the interactions of both non-ionising and directly ionising (i.e. charged) particles (e.g. the Bragg–Gray cavity principle) as will be made clear in Chapter 6. At the microdosimetric level, a fundamental understanding of the action of radiation on cells can only come through studying the track structure of particle tracks in relation to the relevant targets (i.e. the DNA in the cell nucleus). Again, this requires knowledge of the charged-particle interactions. Perhaps the only use of radiation in radiotherapy that does not rely heavily on charged particle interactions is imaging by diagnostic x-rays.

In this chapter, the emphasis is on electrons. However, much of the material applies with little modification to protons and other ions, and this will be indicated where appropriate. There are primarily three interaction mechanisms of importance for electrons in the energy range from a few hundred eV up to 50 MeV*: first, *collisions* with bound atomic electrons (Møller scattering); second, *bremsstrahlung* or radiative losses; and third, *elastic scattering* largely because of the heavy, positively charged nucleus. For heavy particles only (inelastic) collision losses and elastic scattering are important (see Chapter 47 and Chapter 49). In all cases, the consequences of the interactions are twofold: modifications of the incident (direct or secondary) charged particles in terms of energy loss and direction, and transfer of energy to matter, resulting in energy absorption and dose deposition. This second issue will be considered in more detail in Chapter 6.

3.2 COLLISION LOSSES

3.2.1 THEORY

Coulomb interactions with the bound atomic electrons are the principal way that charged particles (electrons, protons, etc.) lose energy in the materials and energies of interest in radiotherapy. The particle creates a trail of ionisations and excitations along its path. Occasionally, the energy transfer to the atomic electron is sufficient to create a so-called *delta ray* (or δ-ray)

* See Section 5.4 for some historical references related to the fundamental electrons and positrons interaction processes.

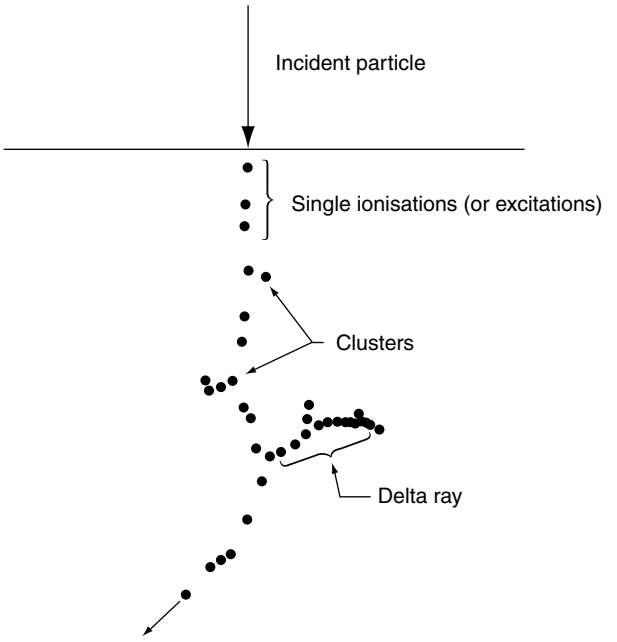

FIGURE 3.1
Diagrammatic representation of the track of a charged particle in matter. (From ICRU, *Linear Energy Transfer, Report 16*, ICRU, Bethesda, MD, 1970.)

which is a (secondary) electron with an appreciable range of its own. This is schematically illustrated in Figure 3.1. A fuller and very readable account of the theory of inelastic collisions between fast charged particles and atomic electrons can be found in Evans (1955).

The physical model of the Coulomb interaction between the fast charged particle and a bound electron in the medium is shown in Figure 3.2. The electron is assumed to be free, and its binding energy assumed to be negligible compared to the energy it receives. The primary particle imparts a net impulse to the bound electron in a direction perpendicular to its path.

Using classical, non-relativistic collision theory, as Bohr once did, from Newton's second law, (i.e. the change in momentum is equal to the impulse [the time integral of the force]) and from the Coulomb law for the force between charged particles, it can be shown that the energy transfer Q is given by:

$$Q = \frac{2k^2z^2e^4}{mb^2v^2} \tag{3.1}$$

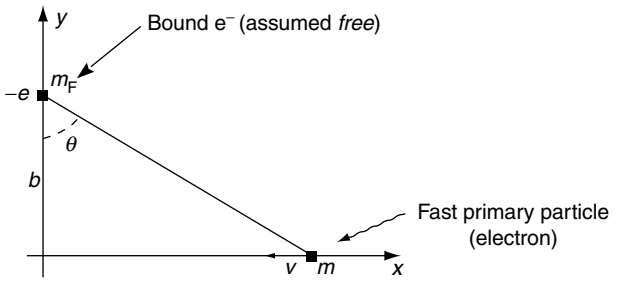

FIGURE 3.2
Interaction between a fast primary charged particle and a bound electron. The incoming electron is moving at a speed v in a direction opposite to axis x. (From Nahum, A. E., *The Computation of Dose Distributions in Electron Beam Radiotherapy*, Medical Physics Publishing, Madison, WI, 1985.)

where b, the distance of closest approach, is known as the *impact parameter*; m is the mass of the electron; z is the charge on the primary particle (in units of the electronic charge e); v is the velocity of the primary particle; and the constant, k, is defined below. It should be noted that the mass of the primary particle does not enter into Equation 3.1, which equally applies to electrons, protons (that both have $z=1$), and other heavier charged particles (see Chapter 46 and Chapter 49). Equation 3.1 leads to the following classical expression for the cross-section per electron, differential in the energy transfer Q:

$$\frac{d\sigma}{dQ} = \frac{2\pi z^2 e^4 k^2}{mv^2}\frac{1}{Q^2} \tag{3.2}$$

The full relativistic, quantum-mechanical cross-section for Coulomb interactions between free electrons, due to Møller (1932), is:

$$\frac{d\sigma}{d\varepsilon} = \frac{2\pi e^4 k^2}{Tm_e v^2}\left[\frac{1}{\varepsilon^2} + \frac{1}{(1-\varepsilon)^2} + \left(\frac{\tau}{\tau+1}\right)^2 - \frac{2\tau+1}{(\tau+1)^2}\frac{1}{\varepsilon(1-\varepsilon)}\right] \tag{3.3}$$

where

T is the electron kinetic energy (k.e.)
$\varepsilon = Q/T$ is the energy transfer in units of the electron k.e.
$\tau = T/m_e c^2$ is the k.e. in units of the electron rest mass
v is the electron velocity
$k = 8.9875 \times 10^9$ Nm^2 C^{-2} (constant appearing in the Coulomb-force expression)

The first term in Equation 3.3 dominates. Ignoring the remaining terms and changing the variable from ε to the energy transfer Q, the classical result given above (Equation 3.2) is obtained. The $1/Q^2$ dependence clearly demonstrates that small losses predominate; the average energy loss in low atomic-number materials is of the order of 60 eV (ICRU 1970). The Møller expression (Equation 3.3) is valid provided that the electron energy is much greater than the binding energies of the atoms in the medium. The binding energies also set a lower limit to the energy transfer possible (see Section 3.2.2).

The terms *soft* and *hard* are often used to describe the different types of collisions. So-called *soft* collisions are said to occur when the fast particle passes an atom at a relatively large distance, and the Coulomb force field affects the atom as a whole, distorting it, with possibly an excitation or ionisation of a valence-shell (i.e. outer) electron. Only a small amount of energy can be transferred of the order of eV. These soft collisions are by far the most numerous type of collision. Cerenkov radiation can result from soft collisions (see Attix 1986); it is entirely negligible as a fraction of the total energy lost in soft collisions. The density or polarization effect is also concerned with soft or distant collisions (see Section 3.2.3).

When the fast particle passes relatively close to the atom (i.e. of the order of the atomic dimensions), then one can properly speak of an interaction with a single bound electron (Figure 3.2). Such hard collisions result in electrons being ejected with appreciable kinetic energy, and these are known as *knock-on* electrons or δ-rays. Hard collisions are naturally much rarer than soft ones, but the contributions of hard and soft collisions to the total energy loss are comparable in magnitude.

If an inner-shell electron is ejected as a result of a hard collision, then the atom will return to its ground state either by the emission of characteristic x-rays or by Auger electrons in the same manner as for the photoelectric effect (see Section 4.3.1).

3.2.2 Collision Stopping Power

The occurrence of very frequent, small energy losses along the path of any charged particle in matter (in marked contrast to the way that photons transfer energy, see Chapter 4) leads

naturally to the concept of *stopping power*, defined as the average energy loss, dE, per unit distance, ds, along the track of the particle. This is usually expressed as the *mass* collision stopping power, written $(1/\rho)(\mathrm{d}E/\mathrm{d}s)_{\mathrm{col}}$ or S_{col}/ρ, which is calculated from

$$\frac{1}{\rho}\left(\frac{\mathrm{d}E}{\mathrm{d}s}\right)_{\mathrm{col}} = N_{\mathrm{A}}\left\langle\frac{Z}{A}\right\rangle\int_{Q_{\min}}^{Q_{\max}} Q\,\frac{\mathrm{d}\sigma}{\mathrm{d}Q}\,\mathrm{d}Q \tag{3.4}$$

where N_{A} is Avogadro's number, and Z and A have their usual meaning (see Chapter 1). $Q_{\max}$ for an electron with kinetic energy E_0 is equal to $E_0/2$*. Note that strictly $(\mathrm{d}E/\mathrm{d}s)$ is a negative quantity as it expresses energy *loss* not energy *gain* as the distance s increases. However, this negative sign has generally been omitted in what follows.

The evaluation of the minimum energy transfer $Q_{\min}$ represents a major difficulty. The integral for stopping power (Equation 3.4) can alternatively be cast in terms of the impact parameter b and then integrating out to $b = \infty$ yields an infinite stopping power because of the large number of soft collisions at large distances. The first approximate solution to this far from trivial problem is due to Niels Bohr (1913, 1948). Bohr's first attempt at this was in 1913 before he had conceived of quantized energy levels for the atomic electrons. Bohr treated the problem in terms of the *time of collision*, τ, and the natural frequency of the atomic electron, ν, such that the electron, if displaced, oscillated about its natural equilibrium position with a period of $1/\nu$. If the collisions are such that τ ($\approx b/v$ i.e. impact parameter/velocity) is short (i.e. $\tau \ll 1/\nu$), then the electron would behave as though it were free and accept the impulse (corresponding to close collisions). If, on the other hand, the collision time was relatively long, such that $\tau \gg 1/\nu$, then the electron acts as though bound; its orbit is distorted or deformed by the passage of the charged particle, but no net energy transfer takes place. This is sometimes referred to as adiabatic behaviour. Bohr showed that the maximum impact parameter $b_{\max} = 1.123v/2\pi\nu$ and, consequently, a finite energy loss per unit pathlength was obtained that included the geometric mean value $\bar{\nu}$ of the Z individual atomic frequencies that are characteristic of different atoms

$$\left(\frac{\mathrm{d}E}{\mathrm{d}s}\right)_{\text{classical}}^{\text{Bohr}} = \frac{4\pi z^2 e^4}{m_{\mathrm{e}}v^2}NZ\ln\frac{1.123m_{\mathrm{e}}v^3M}{2\pi\bar{\nu}ze^2(M+m_{\mathrm{e}})}\ \text{ergs/cm}$$

where M is the mass of the fast charged particle and N is the number of atoms per unit volume.

The full quantum-mechanical expression for the electron mass collision stopping power (Berger and Seltzer 1964; ICRU 1984a, 1984b) is given by

$$\frac{1}{\rho}\left(\frac{\mathrm{d}E}{\mathrm{d}s}\right)_{\mathrm{col}} = \frac{2\pi r_{\mathrm{e}}^2 m_{\mathrm{e}}c^2 N_{\mathrm{A}}}{\beta^2}\left\langle\frac{Z}{A}\right\rangle\left\{\ln\left[\frac{\tau^2(\tau+2)}{2(I/m_{\mathrm{e}}c^2)^2}\right] + F(\tau) - \delta\right\} \tag{3.5}$$

where

$$F(\tau) = 1 - \beta^2 + [\tau^2/8 - (2\tau+1)\ln 2]/(\tau+1)^2 \tag{3.6}$$

and the extra quantities not defined so far are

$m_{\mathrm{e}}c^2$, rest mass energy of the electron
$\beta = v/c$

* Two electrons are indistinguishable after the collision; therefore, it cannot be determined which was the incident electron. Arbitrarily, *the faster electron after the collision is taken to be the incident one*; this results in $Q_{\max} = T/2$. For heavy particles, it can be shown from kinematics that $Q_{max} = T\{1+(2Mc^2/T)\}/\{1+(M+m_0)^2c^2/2m_0T\}$ (e.g. Evans 1955).

r_e, electron radius ($=e^2/m_e c^2 = 2.818\times10^{-15}$ m)
I, mean excitation energy
δ, density-effect correction (see Section 3.2.3)

The above expression can be somewhat simplified if it is expressed in the virtually universally employed units of MeV cm^2 g^{-1} (ICRU 1984a):

$$\frac{1}{\rho}\left(\frac{dE}{ds}\right)_{col} = 0.1535\frac{1}{\beta^2}\left\langle\frac{Z}{A}\right\rangle\left\{\ln\left[\frac{\tau^2(\tau+2)}{2(I/m_e c^2)^2}\right] + F(\tau) - \delta\right\} \text{ MeV cm}^2\text{ g}^{-1} \tag{3.7}$$

The mean excitation energy or potential, I, is an average of the transition energies E_i weighted by their oscillator strengths f_i according to the following:

$$Z\ln I = \sum_i f_i \ln E_i \tag{3.8}$$

It is effectively the geometric mean of all the ionisation and excitation potentials of the atoms in the absorbing medium; it is, of course, the more exact counterpart of Bohr's mean characteristic frequency that was discussed above. In general, I cannot be derived theoretically except in the simplest cases such as monoatomic gases. Instead, it must be derived from measurements of stopping power or range. The most recent values of I, based largely on experimental data, are given in ICRU (1984b). For example the best current estimate of the I-value for water is 75.0 eV. Generally, the I-value increases as Z increases (see Table 3.1).

The correspondence between classical and quantum-mechanical treatments of the energy loss spectrum is illustrated in Figure 3.3, taken from Evans (1955). The quantity $\sigma(Q)/\sigma_0(Q)$ on the ordinate is the ratio of the effective cross-section to the classical one. I is the effective minimum excitation potential of the sth electron. Q is the adiabatic limit of minimum classical energy transfer to the sth electron when the impact parameter has its maximum effective value. In the quantum-mechanical treatment, the energy losses in soft collisions correspond to a type of resonance phenomenon. The fast incident particle has a finite probability of transferring energy to that particular atom. However, either the energy transferred is zero or it is equal to the

TABLE 3.1

Mean Excitation Energies, I, and Other Quantities Relevant to the Evaluation of the Collision Stopping Power of Selected Human Tissues and Other Materials of Dosimetric Interest

Material	I (eV)	$\langle Z/A\rangle$	Density (g cm^{-3})
Adipose tissue (ICRP)	63.2	0.558468	0.920
Air (dry)	85.7	0.499190	1.205×10^{-3}
Bone, compact (ICRU)	91.9	0.530103	1.850
Bone, cortical (ICRP)	106.4	0.521299	1.850
Ferrous-sulphate dosimeter solution	76.3	0.553282	1.024
Lithium fluoride	94.0	0.462617	2.635
Muscle, skeletal (ICRP)	75.3	0.549378	1.040
Muscle, striated (ICRU)	74.7	0.550051	1.040
Photographic emulsion	331.0	0.454532	3.815
PMMA (lucite, perspex)	74.0	0.539369	1.190
Polystyrene	68.7	0.537680	1.060
Water (liquid)	75.0	0.555087	1.000

Source: Adapted from Nahum, A. E., *The Computation of Dose Distributions in Electron Beam Radiotherapy*, Medical Physics Publishing, Madison, WI, pp. 27–55,1985. With permission; Data taken from ICRU (International Commission on Radiation Units and Measurements), Report 37, *Stopping Powers for Electrons and Positrons*, ICRU, Bethesda, MD, 1984. With permission.

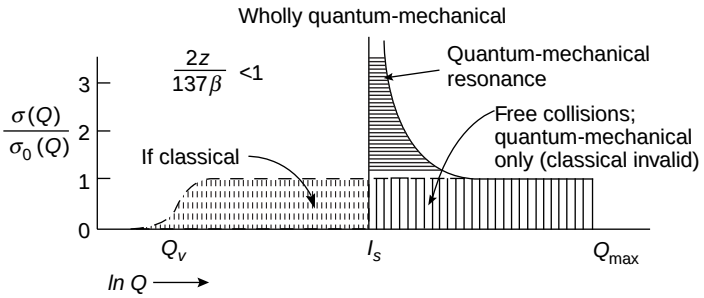

FIGURE 3.3
The ratio of the effective cross-section $\sigma(Q)$ to the classical one $\sigma_0(Q)$ for high particle velocities. The classical theory predicts too large an energy loss as the adiabatic limit, Q_v, becomes much smaller than the allowed minimum energy loss, I_s, as β increases. (From Evans, R. D., *The Atomic Nucleus*, McGraw Hill, New York, 1955. With permission.)

excitation or ionisation energy of the atom. Therefore, quantum mechanics replaces the classical multitude of small losses to each of the atoms by larger losses to only a few of the atoms.

The essential features of the mass collision stopping power are retained in the following simplified expression:

$$\frac{S_{\text{col}}}{\rho} \propto \left\langle \frac{Z}{A} \right\rangle \frac{1}{v^2} [f(\tau) - 2 \ln I - \delta] \tag{3.9}$$

Comparing this expression with Equation 3.5 or Equation 3.7, the increase at decreasing sub-relativistic energies due to the $(1/v^2)$ factor can be identified. This is simply explained by the fact that *slow* electrons spend more time going past an atom than do *fast* ones, and consequently the impulse (see above) is greater and thus more energy is lost. At relativistic energies, there is a more gradual increase in the stopping power which is known as the *relativistic rise*. Figure 3.4 illustrates these two main features.

The explanation for the relativistic rise in stopping power is as follows. The electric field of the moving primary particle undergoes a *Lorentz contraction* at relativistic energies. In the forward and backward directions the field is *weakened* by the factor γ whereas in the transverse directions it is *strengthened* by the factor γ (see footnote); the field-line pattern is changed from spherical to *pancake*-shaped. This *contraction* means that the field of the moving particle acts on the bound atomic electrons for a shorter time (i.e. the collision time, τ, is reduced). Following Bohr's reasoning, this leads to an increase in $b_{\max}$*. The net result of a decrease in τ, a lateral broadening of the field, and an increase in the maximum impact parameter is an increase in the stopping power, approximately logarithmic with energy, as v approaches c, as illustrated in Figure 3.4.

3.2.3 Density Effect

The density or polarization effect (Fermi 1940; Sternheimer 1961; ICRU 1984a) reduces the value of S_{col} at relativistic energies in condensed media via the term δ in Equation 3.5 and Equation 3.9. It is connected to the relativistic rise in the stopping power. The increase in the maximum value of the impact parameter, $b_{\max}$, discussed in the previous section, implies an increase in the volume of the cylinder around the path of the fast charged particle where energy transfers are possible. However, if the stopping medium has a high density, (i.e. condensed media as opposed to gases) then the electric field seen by the atoms distant from the fast particle track is reduced due to the polarization of the intervening atoms (as illustrated in Figure 3.5). Consequently, the contribution of these distant collisions to the stopping power will be reduced.

* $b_{\max}$ increases by the factor $\gamma = 1/\sqrt{1 - v^2/c^2}$.

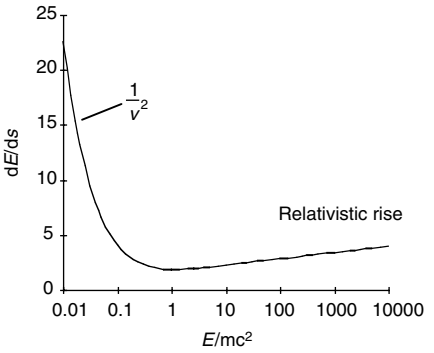

FIGURE 3.4
Collision energy loss as a function of (log) electron kinetic energy (in units of electron rest mass). (From Nahum, A. E., *The Computation of Dose Distributions in Electron Beam Radiotherapy,* Medical Physics Publishing, Madison, WI, 1985.)

This reduction in collision stopping power is known as the *polarization* or *density effect*. Fermi (1940) gave the first theoretical treatment. Sternheimer (1961) subsequently worked out the theory in more detail and gave numerical recipes to calculate the correction factor δ for a number of different materials.

The density effect is of particular importance in the dosimetry of megavoltage electron and photon beams as will become apparent when the water-to-air stopping-power ratio is discussed in Section D.1 of Appendix D. Figure 3.6 shows the variation of S_{col}/ρ with energy for air and water, two substances with similar atomic compositions and similar I-values; note that the energy scale is linear, not logarithmic as in Figure 3.4. The relativistic rise in the collision stopping power in the condensed medium is much less pronounced compared to that in the gas because of the density effect. Consequently, the ratio of mass stopping powers, water to air, is strongly energy dependent above around 0.5 MeV. It will be seen in Section 6.7 and Section 18.2.4 that it is precisely this ratio that determines the energy variation of the response (in terms of dose to water) of an ionisation chamber placed in water, and the energy region above 0.5 MeV is precisely the one that is relevant for the megavoltage photon and electron beams used in radiotherapy.

3.2.4 Electron Stopping-Power Data for Substances of Medical Interest

The material-dependent terms in Equation 3.5 are $\langle Z/A \rangle$, the mean excitation energy I, and the density-effect correction δ. Table 3.1 lists the relevant parameters for various human tissues

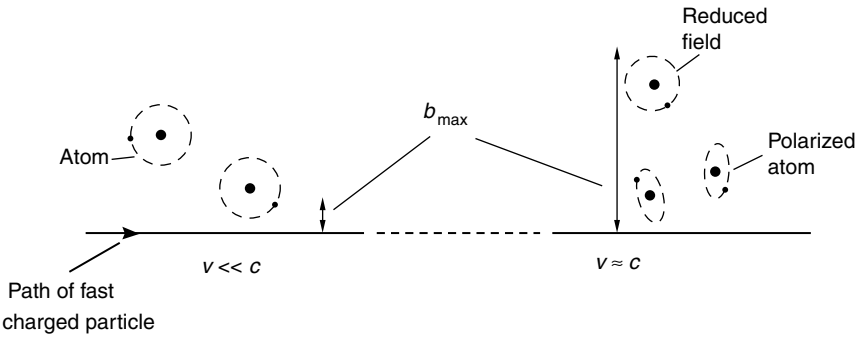

FIGURE 3.5
Schematic explanation of the mechanism of the density (or polarization) effect. (From Nahum, A. E., *The Computation of Dose Distributions in Electron Beam Radiotherapy,* Medical Physics Publishing, Madison, WI, 1985.)

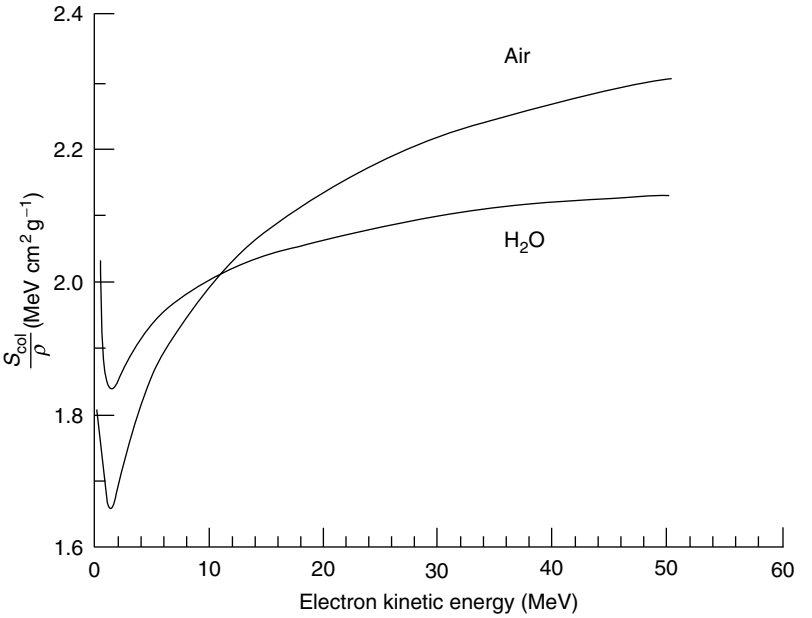

FIGURE 3.6
The variation of mass collision stopping power with electron kinetic energy for air and for water; note the linear energy scale. (From Nahum, A. E., Annual Meeting of the Canadian Association of Physicists, Quebec, 1983.)

and some other substances of dosimetric interest taken from ICRU (1984a) as well as for water as a comparison. It can be seen that the I-values all fall between 73 eV and 75 eV with the exception of adipose tissue (high hydrogen content) and bone with its high calcium content. In fact, the I-value is approximately proportional to the mean atomic number (e.g. the values for aluminium and lead are 166 eV and 823 eV, respectively). Given the similarity of the values of I, $\langle Z/A \rangle$, and the (mass) density (the latter being involved in the density-effect correction δ) in the table, the values of (S_{col}/ρ) must also be very similar. This is very convenient, as it means that the electron energy loss over a given distance in the body can be derived from that in water by simply multiplying by the density, assuming that radiation losses are also very similar, which will generally be the case below around 20 MeV (see Section 3.3.2).

The values of the (mass) stopping-power ratio, $s_{med,air}$, for various substances of interest in medical dosimetry, as a function of electron kinetic energy in the megavoltage region are shown in Figure 3.7. The quantity $\langle Z/A \rangle_{med}/\langle Z/A \rangle_{water}$ has been added along the right hand axis in order to show that for all these substances except bone, where the atomic number is appreciably higher, and air, where the density effect plays the dominant role (see Section 3.2.3), $(S_{col}/\rho)_{med} \propto \langle Z/A \rangle_{med}$ (Equation 3.9). In fact, the curve labelled *Air* also follows this pattern at energies below about 1 MeV where the density effect is negligible. It can also be noted that the ratio is virtually independent of energy except for that of air; this is very convenient for dosimeter response evaluation and treatment planning purposes. These medium-to-water stopping-power ratios are likely to find direct application in the conversion of Monte-Carlo-derived dose distributions in patients (see Chapter 28) to *water-equivalent* doses (Siebers et al. 2000).

3.2.5 Restricted Stopping Power

Use is frequently made of the *restricted stopping power*. This means that only energy transfers below a certain value Δ are included; it is calculated by setting Q_{max} equal to Δ in Equation 3.4. The full expression is again given by Equation 3.5 and Equation 3.6, but with the $F(\tau)$ term now modified to:

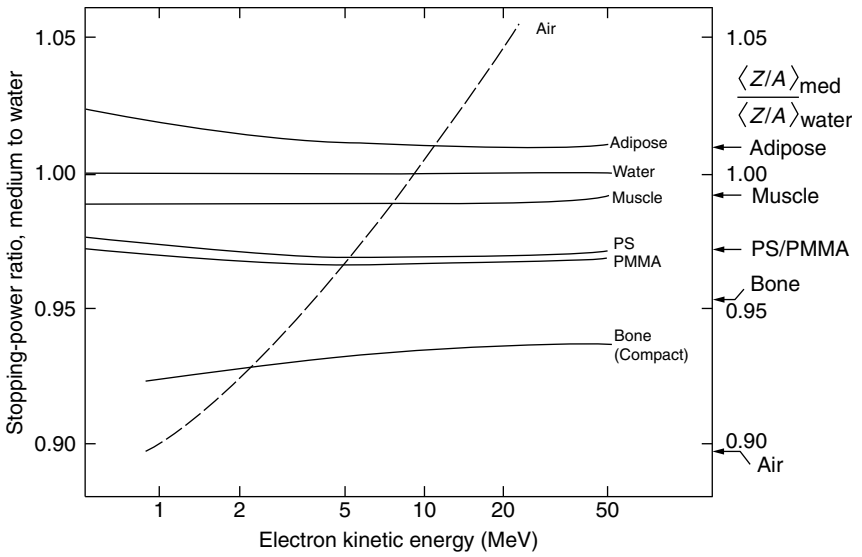

FIGURE 3.7
Ratios of mass collision stopping powers, medium to water, for various substances of medical and dosimetric interest. PS stands for polystyrene and PMMA for polymethyl methacrylate (perspex). The quantity $\langle Z/A\rangle_{\text{med}}/\langle Z/A\rangle_{\text{water}}$ for the various media is given on the right-hand axis. (From Nahum, A. E., *The Computation of Dose Distributions in Electron Beam Radiotherapy*, Medical Physics Publishing, Madison, WI, 1985.)

$$F(\tau,\Delta) = -1 - \beta^2 + \ln\{4\Delta(\tau-\Delta)\tau^{-2}\} + \tau/(\tau-\Delta) + \{\Delta^2/2 + (2\tau+1)\ln(1-\Delta/\tau)\}(\tau+1)^{-2} \tag{3.10}$$

It should be noted that the expression for the restricted stopping power still includes the density-effect correction factor δ (i.e. it is implicitly assumed that all the losses that do not appear because of the density effect are below Δ in energy). This is reasonable as it is precisely the so-called distant (i.e. soft) collisions that are affected by the density effect.

The restricted stopping power is often written L_Δ; it is required in the evaluation of the Spencer–Attix form of the (mass) stopping-power ratio (see Section 6.7.4). The ratio L_Δ/S_{col} as a function of Δ is plotted in Figure 3.8 for 1 MeV and 10 MeV electrons in water; very similar plots would have been obtained for other low-Z substances. The slow decrease from unity with decreasing Δ demonstrates that small energy transfers dominate in the overall energy transfer process as has been previously emphasised.

3.2.6 Collision Stopping Power for Heavy Charged Particles

The stopping-power formula for a singly charged particle heavier than an electron is (Attix 1986; ICRU 1984a)

$$\frac{1}{\rho}\left(\frac{dE}{ds}\right)_{\text{col}} = \frac{2\pi N_A r_e^2 m_e c^2 z^2}{\beta^2}\left\langle\frac{Z}{A}\right\rangle\left\{\left\{\ln\left(\frac{2m_e c^2\beta^2 T'_{\max}}{I^2(1-\beta^2)}\right)\right\} - 2\beta^2 - 2\frac{C}{Z} - \delta\right\} \tag{3.11}$$

where $T'_{\max}$ is the maximum energy that can be transferred in a head-on collision with an (unbound) atomic electron (see footnote). For kinetic energy $T < M_0c^2$, $T'_{\max} \approx 2m_0c^2(\beta^2/1-\beta^2)$*. Following Attix (1986), the above expression can then be

* For a 10 MeV proton, $T'_{\max} = 20$keV; this can be contrasted with a maximum delta ray energy of 5 MeV for a 10 MeV electron.

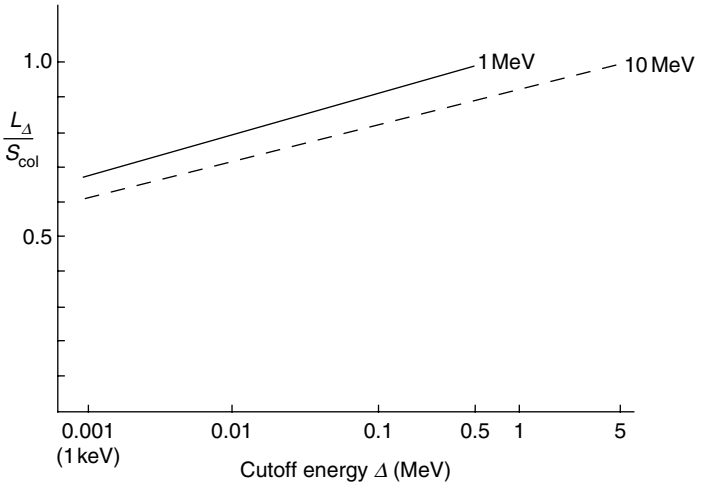

FIGURE 3.8
The ratio of restricted collision stopping power, L_Δ, to unrestricted collision stopping power, S_{col}, for 1 MeV and 10 MeV electrons in water. (From Nahum, A. E., *The Computation of Dose Distributions in Electron Beam Radiotherapy*, Medical Physics Publishing, Madison, WI, 1985.)

simplified to

$$\frac{1}{\rho}\left(\frac{dE}{ds}\right)_{col} = 0.1535\frac{z^2}{\beta^2}\left\langle\frac{Z}{A}\right\rangle\left\{27.675 + 2\ln\left(\frac{\beta^2}{1-\beta^2}\right) - 2\beta^2 - 2\ln I - 2\frac{C}{Z} - \delta\right\} \quad (3.12)$$

Compared to the corresponding formula for electron collision stopping power (Equation 3.6 and Equation 3.7), the above expression contains the so-called shell correction term C/Z. This is necessary as the Born approximation assumption (i.e. $2Zz/137 \ll \beta$) is no longer satisfied when particle velocities approach those of the bound electrons in the stopping medium. K-shell electrons will be affected first as they have the highest (orbital) velocities, then the L-shell and so on. The shell correction approximately accounts for the resulting error in the stopping-power formula. As particle velocities approach those of the various shells, (dE/ds) decreases as those electrons can no longer take part in the energy transfer process. This term may be as large as 10% at low energies, but it is negligible for electrons > 0.1 MeV in energy. The term C/Z is the same for all charged particles of the same velocity. Note that concerning the use of heavy particles in radiotherapy (see Chapter 46 and Chapter 49), the density-effect term δ is almost always negligible as the beam energies necessary for adequate penetration generally fall far short of the relativistic region.

Figure 3.9 compares the collision stopping power in water for protons with that for electrons. It can be seen that the basic shapes are the same, but the proton curve is shifted in energy such that the particle velocities are roughly comparable. Therefore, the minimum for the proton case occurs at around 2000 MeV which is a factor 2000 greater than that for electrons and is basically the ratio of the rest masses.

Heavy charged particles with relatively high energies (100 MeV or greater) can also lose energy through interacting with the nucleus (see Chapter 46 and Chapter 49). This can give rise to neutrons and γ-rays. The magnitude is generally small. As an example, around 2.5% of the energy in a 100 MeV proton beam in a carbon absorber is lost because of nuclear interactions and therefore does not appear as excitations or ionisations (Attix 1986). The effect of nuclear interactions is conventionally not included in the stopping power (or the range) of heavy charged particles. However, in accurate computations of the dose deposited by proton beams, for example using Monte-Carlo simulation, nuclear interactions

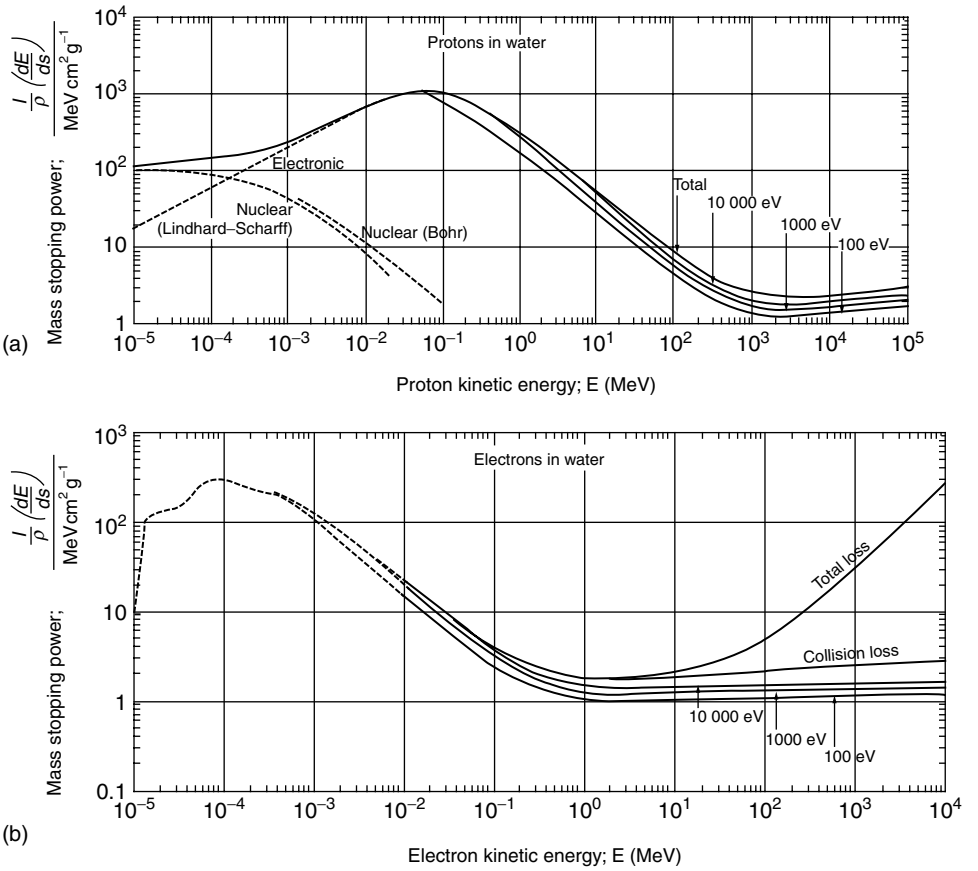

FIGURE 3.9
Mass stopping power in water for protons (a) and electrons (b). Note the similarities in the shapes of the collision stopping power curves, with the minima close to the respected particles' rest mass energies. The curves labelled with energy numbers refer to mass restricted stopping power for different value of Δ—see Section 3.2.5. The curve for the total stopping power (see Section 3.4.1) is also shown. (From ICRU, *Linear Energy Transfer, Report 16*, ICRU, Bethesda, MD, 1970.)

must be taken account of by decreasing the number of particles in the beam as the depth increases; this corresponds to a decrease in the *planar* fluence of the beam with depth (see Section 6.3.5).

3.3 RADIATIVE LOSSES (BREMSSTRAHLUNG)

3.3.1 THEORY

The acceleration of the (very light) electrons in the strong electric field of a nucleus leads to the production of *bremsstrahlung*. The acceleration is proportional to the nuclear charge, Z, divided by the mass, m, of the moving particle (i.e. $\propto Z/m$). The intensity of radiation produced is then proportional to $(Z/m)^2$. One sees immediately that this is a relatively unimportant energy loss mechanism below about 10 MeV in low-Z materials, and it is completely negligible for heavy charged particles. The cross-section, σ_{rad}, for this totally *non-classical* process is extremely complicated. One significant feature is that,

very approximately:

$$\frac{d\sigma_{rad}}{dh\nu} \propto \frac{1}{h\nu} \tag{3.13}$$

Therefore, on average, the losses will be appreciably larger than for collisions (cf. Equation 3.2). This means that one can expect considerable energy-loss straggling due to radiation losses (see Section 3.4.2). Figure 3.10 is a plot of the variation of the product of the differential cross-section (as in the expression above) and the photon energy (i.e. the intensity) with photon energy (expressed as a fraction of the electron kinetic energy) for the case of lead. These curves correspond to the x-ray spectrum that would be produced by monoenergetic electrons beam hitting a thin target, integrated over all directions of the emitted photons.

3.3.2 Radiation Stopping Power

In an exactly analogous fashion to that for collision losses in the previous section, one can define a radiative stopping power, $(dE/ds)_{rad}$ or S_{rad}, and also a mass radiation stopping power (S_{rad}/ρ). The general form of the mass radiative stopping power for high energies (complete screening: $\tau \gg 1/\alpha\, Z^{1/3}$) is given by:

$$(S/\rho)_{rad} = \frac{4r_e^2\alpha}{\beta^2} N_A \frac{Z(Z+1)}{M_A} (\tau+1) m_e c^2 \ln(183Z^{-1/3} + 1/18) \tag{3.14}$$

where α is the fine structure constant ($\alpha \approx 1/137$). From an inspection of Equation 3.14, it can be seen that the radiative stopping power increases almost linearly with kinetic energy

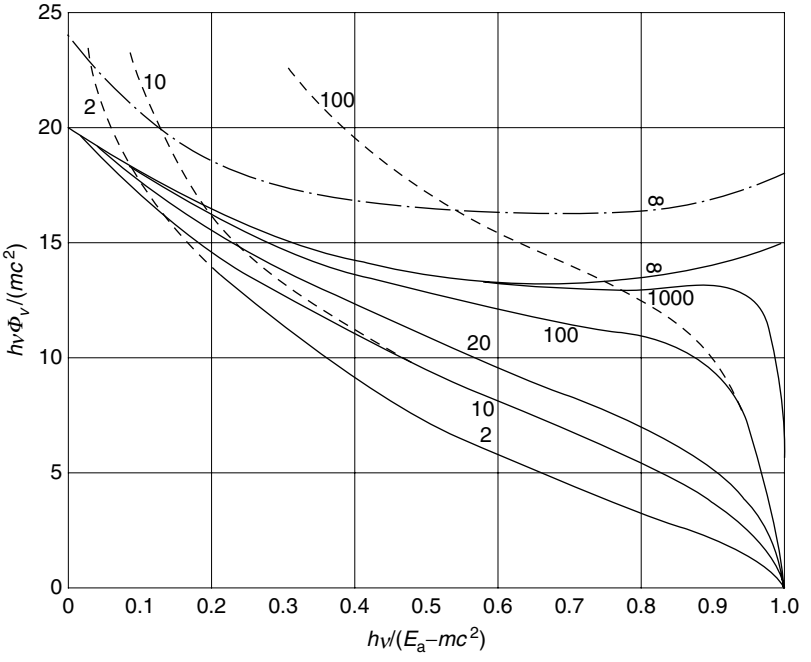

FIGURE 3.10
Energy distribution of the radiation emitted by monoenergetic electrons hitting a thin target. Ordinate—intensity of radiation per unit frequency interval; abcissa—energy of emitted quantum as a fraction of the kinetic energy of the emitting electron. The numbers on the curves indicate the energy of the electron in units of mc^2. Solid curves are for lead, including the effect of screening. Dotted curves are without screening, valid for all Z. (From Evans, R. D., *The Atomic Nucleus*, McGraw Hill, New York, 1955.)

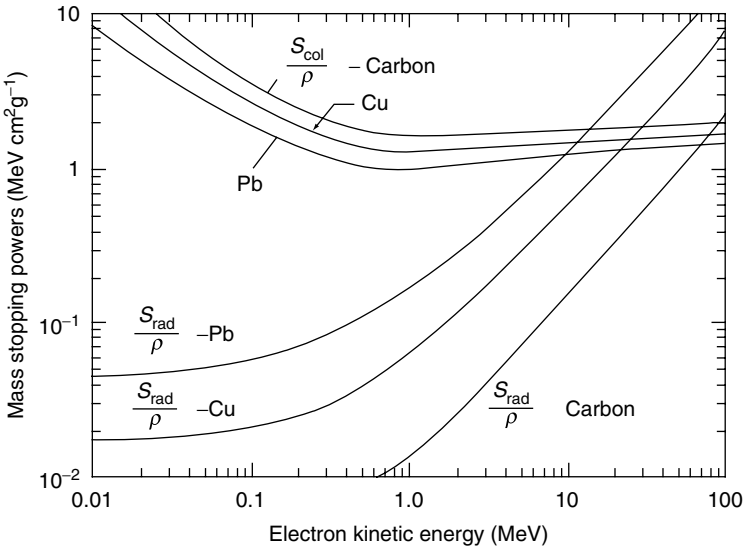

FIGURE 3.11
A comparison of the mass radiative and mass collision stopping powers, S_{rad}/ρ and S_{col}/ρ respectively, for carbon, copper, and lead as a function of the electron kinetic energy. (From Attix, F. H., *Introduction to Radiological Physics and Radiation Dosimetry*, Wiley, New York, 1986.)

in the MeV region, in contrast to the weak logarithmic energy dependence of the collision stopping power (see Section 3.2). Approximately, one can write:

$$\frac{S_{rad}}{\rho} \propto \frac{Z^2}{A} EB \tag{3.15}$$

where B is a very slowly varying function of E and Z. The factor Z^2/A causes an increase in S_{rad}/ρ for higher Z (cf. S_{col}/ρ that decreases slowly with increasing Z). The combined effect of these influences is also evident in Figure 3.11.

From a comparison of Equation 3.9 and Equation 3.14, and also by examining the plots of S_{col}/ρ in Figures 3.4 and 3.9 which show that S_{col}/ρ is approximately constant at the energies where S_{rad}/ρ is non-negligible, it is apparent that $S_{rad}/S_{col} \propto ZE$. A useful quantitative approximation is:

$$\frac{(S_{rad}/\rho)}{(S_{col}/\rho)} = \frac{ZE}{1600 m_e c^2} \tag{3.16}$$

Figure 3.12 illustrates the variation of S_{rad}/S_{col} with electron kinetic energy E for various media of interest in medical dosimetry as well as for aluminium. As the mean atomic number increases, from adipose tissue to bone, S_{rad}/S_{col} increases. It is less than 0.1 below 5 MeV, even for aluminium.

The bremsstrahlung process should be clearly distinguished from the much more frequent *elastic* scattering of charged particles in the Coulomb field of the nucleus that is responsible for almost all the changes in direction of electrons and is dealt with in Section 3.5.

3.3.3 Radiation Yield

A useful quantity is the fraction of the initial electron energy, E_0, that is lost to bremsstrahlung in slowing down to rest. This fraction is known as the *Radiation Yield*, $\Upsilon(E_0)$, and is given by:

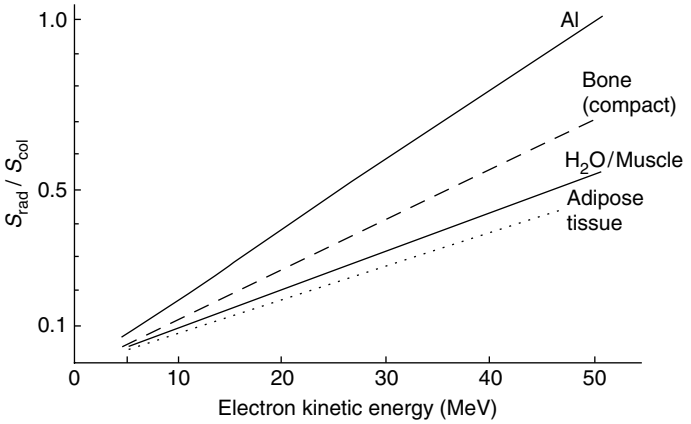

FIGURE 3.12
The energy and material dependence of the ratio of the radiative to the collision stopping power for electrons above 5 MeV. (From Nahum, A. E., *The Computation of Dose Distributions in Electron Beam Radiotherapy,* Medical Physics Publishing, Madison, WI, 1985.)

$$\Upsilon(E_0) = \frac{1}{E_0}\int_0^{E_0} \frac{S_{rad}(E)}{S_{col}(E) + S_{rad}(E)}\,dE \tag{3.17}$$

The dependence of $\Upsilon(E_0)$ on E_0 and on Z is approximately linear, which closely corresponds to the relation between S_{rad}/ρ, E, and Z discussed above.

The radiation yield is involved in calculating the dosimetric quantity, g, which is the fraction of energy transferred (by photons) to a medium in the form of electron kinetic energy that is subsequently re-radiated as bremsstrahlung (see Section 6.3.2).

3.3.4 Angular Distribution of Bremsstrahlung Photons

The angular distribution of the emitted photons is very strongly forward-peaked at relativistic electron energies with a mean value $\theta \approx mc^2/E$ where E is the total energy of the electrons. This forward-peaking is the reason for the flattening filter in a linear accelerator treatment head. It can be noted that, at the much lower electron energies involved in largely diagnostic but also some therapeutic kilovoltage x-ray machines, the angular distribution is much closer to isotropic; hence, the steep angle of x-ray targets (see Section 10.3.1.3).

Chapter 9 in Attix (1986) should be consulted for more details on all aspects of the bremsstrahlung process.

3.4 TOTAL ENERGY LOSSES

3.4.1 Total Stopping Power

The potentially confusing convention in this field is to term the inelastic electron–electron Coulomb interactions *collisions*; whereas bremsstrahlung losses are always termed *radiative losses*. The collision and radiative stopping powers are frequently summed to give the total stopping power, written $(dE/ds)_{tot}$ or S_{tot}:

$$\left(\frac{dE}{ds}\right)_{tot} = \left(\frac{dE}{ds}\right)_{col} + \left(\frac{dE}{ds}\right)_{rad} \tag{3.18}$$

or

$$S_{tot} = S_{col} + S_{rad}$$

Figure 3.9b shows the total mass stopping power (labelled "Total Loss"), mass collision stopping power, and several restricted mass collision stopping powers ($\Delta = 10$ keV, 1 keV and 100 eV) for water against electron kinetic energy E for values between 10^{-5} MeV and 10^{4} MeV. It can be seen that $(S/\rho)_{tot}$ varies slowly with E over the energy range of primary interest in radiotherapy (from 1.937 MeV cm^2 g^{-1} at 4 MeV to only 2.459 MeV cm^2 g^{-1} at 25 MeV).

Several features should be noted:

- Radiation losses only become important above around 10 MeV in water
- The relativistic rise in the collision losses is small because of the density effect
- Collision losses restricted to $\Delta < 10$ keV only result in a modest reduction in stopping power compared to the unrestricted S_{col} which emphasizes the predominance of very small losses
- The approximate value for the electronic stopping power in water in the MeV region is around 2 MeV cm^{-1}; the value in tissue is very similar.

3.4.2 Energy-Loss Straggling

It is important to realize that stopping power is an average value for the energy loss per unit distance. Fluctuations will occur about this mean value in any real situation. This gives rise to what is known as *energy-loss straggling*. Figure 3.13 illustrates the idea; E_0 is the electron energy incident on a thin absorber and the distribution of electron energies emerging from the foil are shown where ΔE_{tot} would be predicted by the product of the thickness of the absorber and the (total) stopping power, S_{tot}. The width Γ is related to the distribution of the individual energy losses. If all energy loss is much smaller than the electron kinetic energy, then Γ will be narrow. This implies that most of the straggling results from the rare, large-energy losses (see Berger and Wang 1988 for a more in-depth treatment).

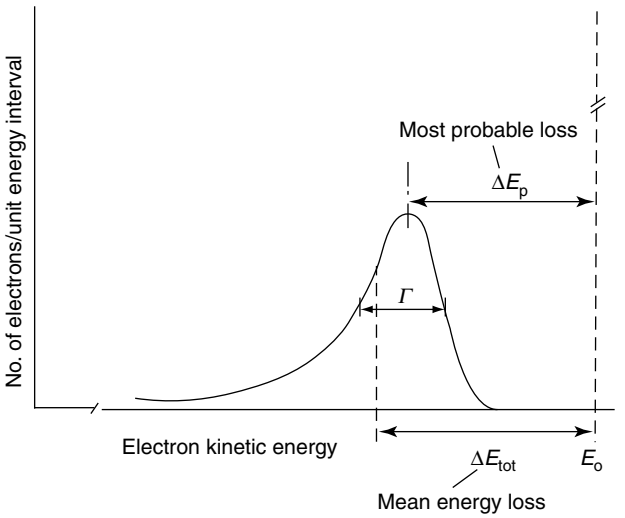

FIGURE 3.13
Energy broadening because of energy-loss straggling after the passage of a monoenergetic electron beam (energy E_0) through a thin absorber. (From Nahum, A. E., *The Computation of Dose Distributions in Electron Beam Radiotherapy,* Medical Physics Publishing, Madison, WI, 1985.)

3.4.3 Continuous-Slowing-Down-Approximation (CSDA) Range

Charged particles lose energy in a quasi-continuous fashion along their tracks in matter, eventually coming to rest. This means that, unlike photons with their exponential attenuation (see Chapter 4), charged particles do have a finite, reasonably well-defined range. Mathematically it has been found convenient to define the so-called continuous-slowing-down-approximation (csda) range, r_0 in the following fashion:

$$r_0 = \int_0^{E_0} \frac{1}{S_{\text{tot}}(E)} \, \mathrm{d}E \tag{3.19}$$

This represents the average pathlength travelled in coming to rest by a charged particle having kinetic energy, E_0. Note that for electrons, as opposed to heavy charged particles, this will always be considerably greater than the average penetration depth because of the marked angular deflections that electrons suffer in slowing down (see Section 3.5). The csda range r_0 is approximately proportional to E_0 in the therapeutic energy range because of the relatively slow variation of S_{tot} in this energy range (see Figure 3.9b). The quantity $r_0\rho$ is analogous to the mass stopping power, (S/ρ), and has the units of mass per unit area (e.g. g cm^{-2}). Other definitions of electron range of particular use in radiotherapy with electron beams, such as the practical range, R_{p}, and R_{50}, are discussed elsewhere in the book (see Section D.3.2 and Section 24.1).

3.4.4 Tabulated Stopping-Power Data

ICRU (1984a) provides total mass stopping powers, mass collision stopping powers, mass radiative stopping powers, csda ranges, radiation yields, and density-effect corrections for electrons for a very wide range of materials, including many of interest in radiotherapy dosimetry. A selection of stopping-power and range data can be found in Tables M.2, at the end of this book.

3.5 ELASTIC NUCLEAR SCATTERING

When a charged particle passes close to the atomic nucleus, at a distance much smaller than the atomic radius, the Coulomb interaction will now be between the fast particle and the nuclear charge rather than with one of the bound electrons (see Section 3.2). In the case of electrons, this causes appreciable changes of direction, but almost never (with the exception of the bremsstrahlung process—see Section 3.3) any change in energy. The scattering is basically *elastic*, the energy lost being the negligible amount required to satisfy momentum conservation between the very light electron and the positively charged nucleus (at least two thousand times heavier). Figure 3.14 gives an indication of the importance of this process which accounts for almost all the changes in electron direction.

This interaction process is essentially Rutherford scattering with differential cross-section:

$$\frac{\mathrm{d}\sigma}{\mathrm{d}\theta} = \frac{\pi e^4 Z^2 (1-\beta^2)}{2m^2 v^4} \frac{\sin\theta}{\sin^4(\theta/2)} \tag{3.20}$$

A correction for screening is essential to prevent the cross-section from becoming infinite when integrated over all angles. A more accurate cross-section that accounted for electron spin was later derived by Mott (see Berger and Wang 1988).

In order to be able to treat the very large number of (single) scatterings occurring in even thin absorbers, analytical theories for multiple scattering (i.e. the combined effect of many

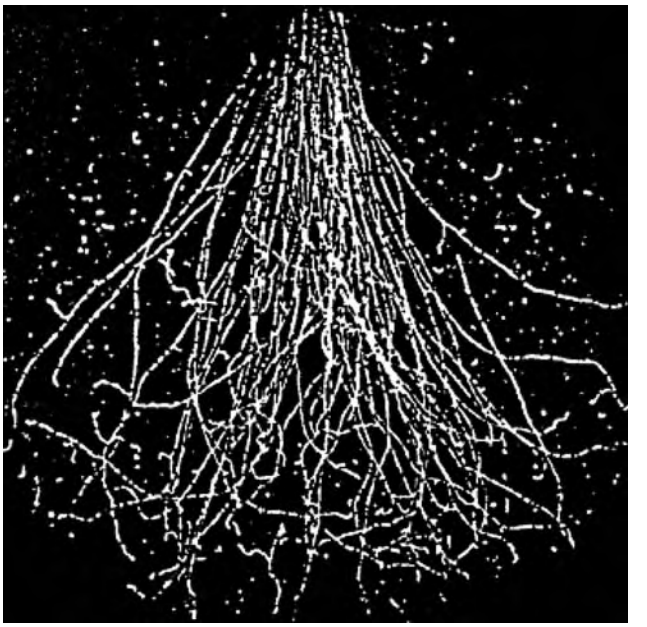

FIGURE 3.14
Bubble chamber picture of a narrow 9.3 MeV electron beam in propane. The increasing multiple scatter toward the end of the electron range is clearly seen. (From Harder, D., Harigel, G., and Schultz, K., *Strahlentherapie,* 115,1, 1961.)

individual single-scattering events) were developed (Rossi 1952; Andreo 1985; Berger and Wang 1988; Fernández-Varea et al. 1993). The simplest multiple scattering theory, though of limited accuracy, is the Gaussian small-angle one (Rossi 1952) that can be expressed as

$$P(\theta)\mathrm{d}\theta = \frac{2}{\overline{\theta^2}}\theta \exp\left(-\frac{\theta^2}{\overline{\theta^2}}\right)\mathrm{d}\theta \tag{3.21}$$

which is the probability of finding an electron with a direction between θ and $\theta + \mathrm{d}\theta$ after traversal through an absorber. The mean square scattering angle, $\overline{\theta^2}$, is given by the product of the absorber thickness, s, and the scattering power, defined as $(\mathrm{d}\overline{\theta^2}/\mathrm{d}s)$ and usually (and somewhat confusingly cf. kinetic energy) denoted by T:

$$\overline{\theta^2} = s\left(\frac{\mathrm{d}\overline{\theta^2}}{\mathrm{d}s}\right) = sT \tag{3.22}$$

The quantity scattering power is analogous to stopping power. The mass scattering power is similarly written T/ρ. It increases with decreasing electron energy and increasing atomic number. Scattering power is dealt with in detail in Kase and Nelson (1978) and in ICRU (1984a) which gives tables of T/ρ for materials and energies of relevance in dosimetry. Li and Rogers (1994) should be consulted for an excellent discussion of the validity and application of the concept of electron mass scattering power.

Following Rossi (1952) and Kase and Nelson (1978), through the superposition of small and independent events, the mass scattering power (expressed for instance in radians^2 cm^{-1}) is given by

$$\frac{1}{\rho}\frac{\mathrm{d}\overline{\theta^2}}{\mathrm{d}s} \equiv T = \frac{N_0}{A}\int_{\theta_1}^{\theta_2} \theta^2 \frac{\mathrm{d}\sigma}{\mathrm{d}\omega}\mathrm{d}\omega \tag{3.23}$$

which becomes

$$\frac{T}{\rho} = 16\pi N_0 \frac{Z^2}{A} r_0^2 \left(\frac{mc^2}{p\beta c}\right)^2 \ln[196(Z/A)^{1/6} Z^{-1/3}] \tag{3.24}$$

where the Rutherford single-scattering cross-section has been used (Equation 3.20), p is the electron momentum, the screening angle θ_1 is given by $\alpha Z^{1/3}(m/p)$, the large-angle limit θ_2 by $280\ A^{-1/3}\ (m/p)$, and the small-angle assumption $\sin\theta \approx \theta$ has been made. Equation 3.24 illustrates the dependence of T/ρ on the electron kinetic energy and on Z.

An idea of the magnitude of electron scattering in low-atomic number materials is given in Figure 3.15, where the Gaussian multiple-scattering distribution (Equation 3.21) has been evaluated in the framework of small-angle Fermi–Eyges transport theory (Chapter 27) for 11.8 MeV electrons in water.

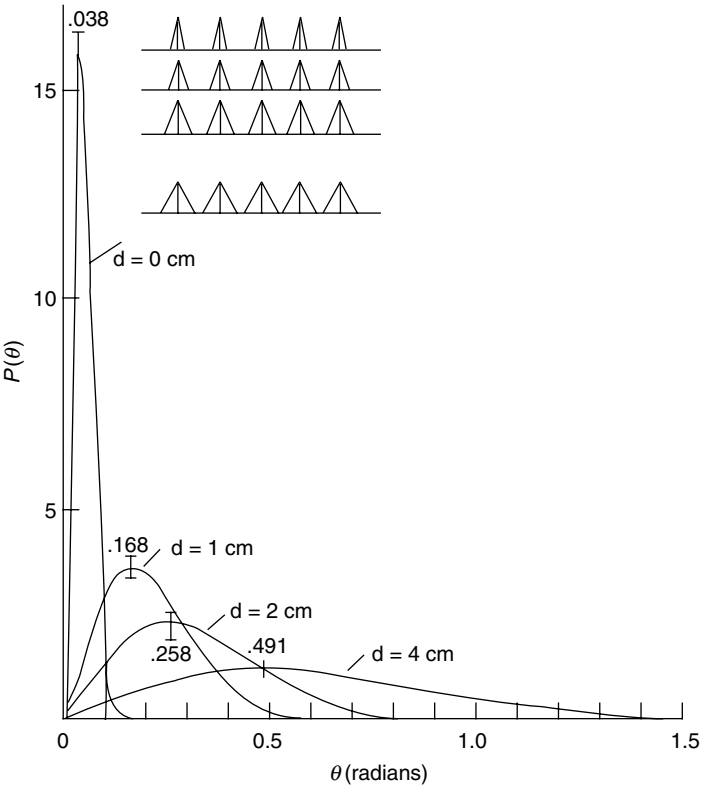

FIGURE 3.15
The angular distribution of electrons (E_0 = 11.8 MeV) vs. depth, d, in water based on Fermi–Eyges transport theory which uses simple Gaussian multiple scattering; note that a small angular spread was assumed at the surface. (From Hogstrom, K. R. and Almond, P. R., *The Effect of Electron Multiple Scattering on Dose Measured in Non-Water Phantoms*, AAPM Annual Meeting, 1982.)

3.6 APPLICATION TO AN ELECTRON DEPTH–DOSE CURVE

Figure 3.16 illustrates the physics of electron interactions as they apply to electron beams used in radiotherapy (see also Nahum and Brahme 1985); it shows three different depth–dose curves obtained through Monte-Carlo simulation (see Chapter 5), corresponding to different approximations about electron transport physics for a 30 MeV broad, monoenergetic, and parallel electron beam in water (see also Section 24.2 for a detailed description of electron depth–dose curves).

The curve labelled "CSDA straight ahead" corresponds to straight tracks and shows the Bragg Peak, normally associated with heavy charged particles (see Chapter 46); this extremely simple approximation illustrates very clearly the behaviour of the total stopping power S_{tot} as the electron energy gradually decreases with depth (see Section 6.6 for the relation between absorbed dose, electron fluence, and mass stopping power). The gradual decrease in dose with depth mirrors the decrease in total stopping power with falling electron energy. At an energy close to that of the electron rest mass (0.511 MeV), however, the collision stopping power goes through a minimum and then rises rapidly (principally because of the $1/\beta^2$ term in Equation 3.5.

The "CSDA multiple scattering" curve involves directional changes through multiple scattering (Equation 3.20 through Equation 3.23), but does not involve any secondary particle transport or any simulation of energy-loss straggling (see Section 3.4.2). The increase in dose away from the surface is entirely due to the increasing average obliquity of the electron tracks with depth and the fact that the beam is *broad* (i.e. there is lateral scattering equilibrium); this is

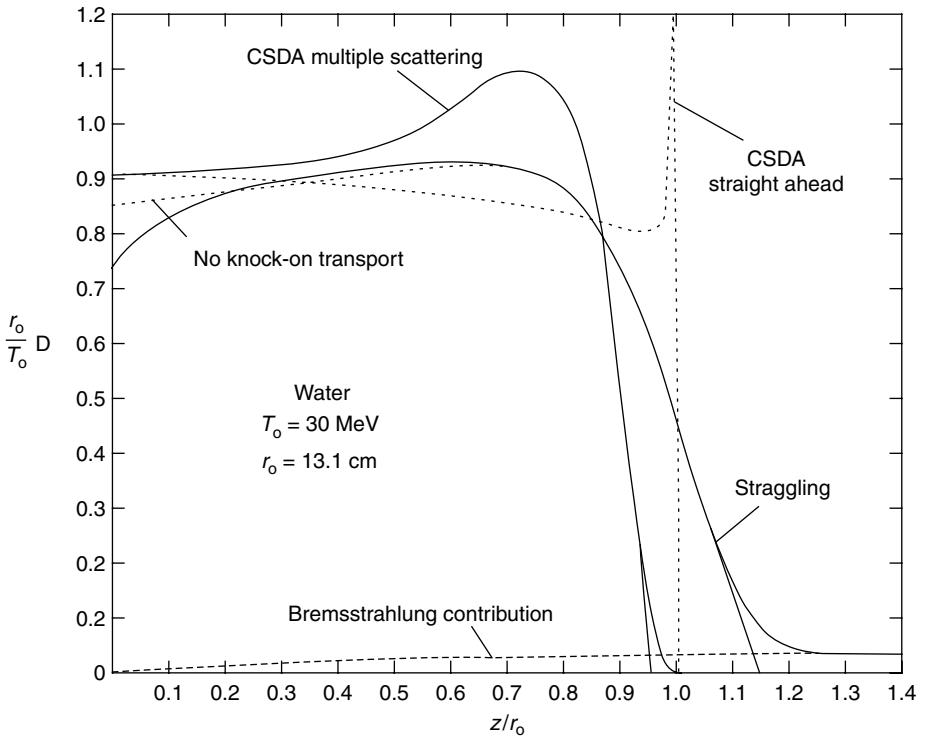

FIGURE 3.16
The effect of various approximations on the electron depth-dose curve for a broad, 30 MeV electron beam in water (csda range $r_o = 13.1$ cm), illustrating the physics of electron interactions covered in this chapter. (From Seltzer, S. M., Hubbel, J. H., and Berger, M. J., *National and International Standardization of Radiation Dosimetry*, Vol. 2, IAEA, Vienna, 1978.)

sometimes known as *scatter buildup*). At around $z/r_0 = 0.7$, the planar fluence (see Section 6.3.5) starts to decrease as electron tracks begin to reach their end. The maximum occurs as a result of a competition between the scatter build-up and the decrease in the planar fluence because of electrons reaching the end of their range.

The "No knock-on transport" curve does not include the generation and transport of knock-on electrons or delta rays, but it does include radiative losses (i.e. bremsstrahlung [see Section 3.3]) and one sees the so-called *bremsstrahlung tail* beyond the practical range. Also, now the slope of the dose falloff is much reduced; this is primarily due to the incorporation of energy-loss straggling (see Section 3.4.2). Finally, the unlabelled full curve corresponds to a simulation including the full electron transport physics (of most relevance in this energy region). The effect of simulating δ-ray transport is clearly seen in the build-up close to the surface; this is analogous to the much more pronounced one in megavoltage photon beams where the ranges of the mainly Compton electrons are significantly greater than those of the predominantly low-energy δ-rays.

In the case of heavy charged particles, the depth-dose curve (for a broad, approximately parallel beam) has a totally different appearance. The well-known Bragg Peak is the most prominent feature; in fact, this is the reason why proton beams are so well-suited to radiotherapy (see Chapter 46). In marked contrast to electron beams, the angular deflections in this case are much less pronounced due to these particles being at least 2000 times more massive than electrons. Consequently, all heavy-particle tracks are approximately straight except at the very end of their range; therefore, the appearance of depth-dose (and the fluence) curves most resembles that labelled "CSDA straight ahead" in Figure 3.16. Furthermore, there is negligible bremsstrahlung, and consequently much less energy-loss straggling, and also a gradual *increase* in the stopping power and hence the dose with decreasing (sub-relativistic) particle kinetic energy (i.e. increasing depth).